

Monte-Carlo simulation of nano-collected current from a silicon sample containing a linear arrangement of uncapped nanocrystals

Mohammed Ledra and Abdelillah El Hdiy

Citation: [Journal of Applied Physics](#) **118**, 115705 (2015); doi: 10.1063/1.4930810

View online: <http://dx.doi.org/10.1063/1.4930810>

View Table of Contents: <http://scitation.aip.org/content/aip/journal/jap/118/11?ver=pdfcov>

Published by the [AIP Publishing](#)

Articles you may be interested in

[The effects of an uncapped nanocrystal on a simulated induced current collected by a nano-contact](#)
 J. Appl. Phys. **117**, 115704 (2015); 10.1063/1.4915281

[Nano-electron beam induced current and hole charge dynamics through uncapped Ge nanocrystals](#)
 Appl. Phys. Lett. **100**, 163117 (2012); 10.1063/1.4705299

[Three-dimensional simulation of electron beam induced current collected by a nano-contact: Diffusion and collection analysis](#)
 J. Appl. Phys. **110**, 124515 (2011); 10.1063/1.3672829

[Electron beam energy and Ge nanocrystal size effects on the minority carrier diffusion length measured by the nano-electron beam induced current technique](#)
 J. Appl. Phys. **110**, 024514 (2011); 10.1063/1.3614527

[Enhanced carrier collection observed in mechanically structured silicon with small diffusion length](#)
 J. Appl. Phys. **86**, 7179 (1999); 10.1063/1.371809


Instruments for Advanced Science

| | | | | |
|----------------------------------------------------------------------------------------------------------------------------------------------------------------------------------------------------------------------------------------------------------------|----------------------------------------------------------------------------------------------------------------------------------------------------------------------------------------------------------------------------------------------------------------------------------------------------------------------------------------------------------------------------------------------|----------------------------------------------------------------------------------------------------------------------------------------------------------------------------------------------------------------------------------------------------------------------------------------------|----------------------------------------------------------------------------------------------------------------------------------------------------------------------------------------------------------------------------------------------------------------------------------------------------------------------------------------|----------------------------------------------------------------------------------------------------------------------------------------------------------------------------------------------------------------------------------------------------------------------------------------------------------------------------------------------------------|
| <p>Contact Hiden Analytical for further details: W www.HidenAnalytical.com E info@hiden.co.uk</p> <p>CLICK TO VIEW our product catalogue</p> |  <p>Gas Analysis</p> <ul style="list-style-type: none"> › dynamic measurement of reaction gas streams › catalysis and thermal analysis › molecular beam studies › dissolved species probes › fermentation, environmental and ecological studies |  <p>Surface Science</p> <ul style="list-style-type: none"> › UHV TPD › SIMS › end point detection in ion beam etch › elemental imaging - surface mapping |  <p>Plasma Diagnostics</p> <ul style="list-style-type: none"> › plasma source characterization › etch and deposition process reaction › kinetic studies › analysis of neutral and radical species |  <p>Vacuum Analysis</p> <ul style="list-style-type: none"> › partial pressure measurement and control of process gases › reactive sputter process control › vacuum diagnostics › vacuum coating process monitoring |
|----------------------------------------------------------------------------------------------------------------------------------------------------------------------------------------------------------------------------------------------------------------|----------------------------------------------------------------------------------------------------------------------------------------------------------------------------------------------------------------------------------------------------------------------------------------------------------------------------------------------------------------------------------------------|----------------------------------------------------------------------------------------------------------------------------------------------------------------------------------------------------------------------------------------------------------------------------------------------|----------------------------------------------------------------------------------------------------------------------------------------------------------------------------------------------------------------------------------------------------------------------------------------------------------------------------------------|----------------------------------------------------------------------------------------------------------------------------------------------------------------------------------------------------------------------------------------------------------------------------------------------------------------------------------------------------------|

Monte-Carlo simulation of nano-collected current from a silicon sample containing a linear arrangement of uncapped nanocrystals

Mohammed Ledra^{1,a)} and Abdelillah El Hdiy^{2,b)}

¹Laboratory of Metallic and Semiconducting Materials, Biskra University, B.P. 145, RP 07000 Biskra, Algeria

²Laboratoire de Recherche en Nanosciences (EA4682), UFR SEN, Université de Reims, Champagne-Ardenne, BP 1039, 51687 Reims Cedex 2, France

(Received 8 June 2015; accepted 30 August 2015; published online 16 September 2015)

A Monte-Carlo simulation algorithm is used to study electron beam induced current in an intrinsic silicon sample, which contains at its surface a linear arrangement of uncapped nanocrystals positioned in the irradiation trajectory around the hemispherical collecting nano-contact. The induced current is generated by the use of electron beam energy of 5 keV in a perpendicular configuration. Each nanocrystal is considered as a recombination center, and the surface recombination velocity at the free surface is taken to be zero. It is shown that the induced current is affected by the distance separating each nanocrystal from the nano-contact. An increase of this separation distance translates to a decrease of the nanocrystals density and an increase of the minority carrier diffusion length. The results reveal a threshold separation distance from which nanocrystals have no more effect on the collection efficiency, and the diffusion length reaches the value obtained in the absence of nanocrystals. A cross-section characterizing the nano-contact ability to trap carriers was determined. © 2015 AIP Publishing LLC. [<http://dx.doi.org/10.1063/1.4930810>]

I. INTRODUCTION

The electron beam induced current (EBIC) is well known as a powerful technique employed to analyze defects and impurities in semiconductor devices. The technique is based on the charge separation by built-in or applied field, which creates the charge collection signals that provide EBIC contrast. The amount of the collected signal depends on the recombination rate of the excess minority carriers as well as the position of the junction with respect to the carrier generation site. This technique is usually used to determine the minority carriers lifetime, diffusion length, surface recombination velocity, and image the electrical activity of defects.^{1–12} However, the progress of nanotechnology makes the conventional EBIC method unsuccessful to give significant and clear information because of its unsatisfactory resolution. Indeed, this resolution is mainly limited by the lateral dimension of the energy dissipation volume, which depends on the studied material and primary electron beam (e-beam). Currently, a powerful experimental method using a nano-contact to collect EBIC, called nano-EBIC, was projected to study nanostructures. Indeed, minority carrier diffusion length and carrier capture efficiency have been studied by this technique on semiconductor structures containing on their surface uncapped germanium (Ge) nanocrystals (NCs).^{13–16} Its very good resolution allows to study, not only the local transport through nanocrystals (NCs) but also the charge retention mechanism in an individual NC.¹⁴ Nevertheless, it is not easy to separate between the free surface and the NCs effects on the evolution of the physical parameters like as the minority carrier diffusion length. This is the major reason of the use of Monte-Carlo (MC) algorithm.^{17–21} Different physical parameters have been analyzed

and their effects have been compared to classical studies to show the difference between standard EBIC and nano-EBIC techniques. For example, the evolution of the minority carrier diffusion length as a function of the e-beam energy has shown a new behaviour.^{19,21} The simulation of the nano-EBIC also allows the extraction of the surface recombination velocities from simulated collection efficiency.²¹

The aim of this work is to study the collection efficiency profile (which controls the evolution of the diffusion length) in the presence of a linear arrangement of uncapped NCs around the nano-contact. These NCs are located in the e-beam irradiation trajectory. The collection efficiency will also be studied as a function of the distance separating each NC from the nano-contact. The analysis of these results leads to understand the NC efficiency to trap carriers. This study is interesting for both information retention in memory devices and recombination effects in optoelectronic devices. Another interesting parameter is the NCs density (d_{NC}). Instead of studying this parameter, we introduce the variation of distance x_{cc} separating two NCs arranged in a linear form with the nano-contact. Indeed, for a given micrometric surface, a decrease of x_{cc} corresponds to an increase of d_{NC} and an increase of x_{cc} means a decrease of d_{NC} . So the additional aim of this study is to analyze the x_{cc} effect on the nano-EBIC collection efficiency in order to describe the NCs density effect.

II. SUMMARIZED MONTE-CARLO ALGORITHM DESCRIPTION

The description of the MC simulation algorithm analyzing standard EBIC is well detailed in many papers.^{22–31} Some previous papers give exhaustive information on the simulated nano-EBIC.^{17–21} The contribution of the present work concerns the simulation of the effect of a linear and

^{a)}Ledra.mohammed@gmail.com

^{b)}abdelillah.elhdiy@univ-reims.fr

symmetric arrangement of two NCs around the nano-contact along the e-beam irradiation trajectory. The nano-contact is regarded as a nanoscale disc at the surface of the studied sample with a hemispherical depletion zone of radius $r_D = 10$ nm. Each of both NCs, behaving as a recombination center, is considered as a disc of radius $r_{NC} = 30$ nm. In this simulation, the distance x_{cc} , separating each NC from the nano-contact center, changes to take into account of the variation of d_{NC} . Indeed, for the scattered surface, an increase (or a decrease) of x_{cc} translates to a reduction (an increase) of the NCs number. Therefore, d_{NC} can be controlled by the parameter x_{cc} . In this study, the effect of the metallic film of the nano-contact is neglected. The sample is irradiated under 5 keV in succession by 200 electrons one after another at a given position x along the e-beam irradiation trajectory over a given length on either side of the nano-contact. A schematic representation of the nano-EBIC procedure is given in Fig. 1. The energy lost by a primary electron between two successive collisions creates n_{gi} electron-holes pairs. The nano-EBIC was obtained by simulating the random diffusion and collection of the minority carriers that are generated at punctual sources randomly distributed within the generation volume. The dependence of the simulated nano-EBIC collection efficiency profiles upon the distance x_{cc} between the two NCs is analyzed. The free surface is characterized by a recombination velocity equal to zero. In this case, the charge, emerged at the surface, diffuses along a random trajectory, where it can be collected by the nano-contact or to be recombined if it reaches one of both nanocrystals otherwise it continues to diffuse along a random trajectory at the free surface or towards the bulk of the sample. In the bulk, the carrier is assumed to be recombined after a given number of diffusion steps or it can be collected when it reaches the depletion region. The bulk diffusion length value is fixed at $L_B = 1 \mu\text{m}$, which was experimentally determined at 5 keV.¹⁵ For each position x of incident primary e-beam, the simulated nano-EBIC collection efficiency $\eta(x)$ is given by

$$\eta(x) = \frac{\sum_{i=1}^{N_s} n_{ci}}{\sum_{i=1}^{N_s} n_{gi}}, \quad (1)$$

where n_{ci} and n_{gi} are, respectively, the number of collected and generated minority carriers for each source S_i whose coordinates are x_i, y_i, z_i , and N_s is the total number of

punctual sources. The value $x = 0$ corresponds to the position of the normal e-beam on the top of the nano-contact center.

III. RESULTS AND DISCUSSIONS

As a reminder, for the calculation, the primary electron energy is kept at 5 keV, the total number of the primary electrons is fixed at 200 electrons, and all other physical parameters (the bulk minority carrier diffusion length, the nano-contact, the nano-depletion zone and NCs sizes) are kept constant. Only the distance x_{cc} separating both NCs from the nano-contact center changes between successive scattering to highlight its effect on the nano-EBIC collection efficiency $\eta(x)$ profiles and their maximum η_{max} . The variation of x_{cc} represents the variation of d_{NC} . The evolution of the η_{max} represents the carriers collection efficiency at the nano-contact center, and the $\eta(x)$ profile controls the minority carrier diffusion length. Therefore, this study allows description of the NCs aptitude to control both carrier transport and storage.

Typical results of $\eta(x)$ obtained by our algorithm are given in Figures 2(a) and 2(b), which show three profiles, the higher corresponds to the case of the NCs absence, and the others describe the $\eta(x)$ profile in the presence of two NCs symmetrically localized around the nano-contact along the e-beam irradiation trajectory at $x_{cc} = 100$ nm and $x_{cc} = 500$ nm, respectively. The results show two essential observations. First, $\eta(x)$ is higher in the case of the NCs absence than in their presence at the surface of the studied sample. This is not surprising because carriers recombination process at the free surface is absent (or at least negligible), since the recombination velocity is taken equal to zero. Second, the variation of x_{cc} parameter effect on the nano-EBIC profile is emphasized; the collection efficiency $\eta(x)$ is higher for $x_{cc} = 500$ nm than for $x_{cc} = 100$ nm. Moreover, as shown in Fig. 2(b), in the area close to the nano-contact $\eta(x)$ corresponding to $x_{cc} = 500$ nm is superimposed to that obtained in the absence of the NCs.

When the recombination centers (here both NCs) are close to the collecting nano-contact, the collected current decreases because of the competition between the carrier collection by the nano-contact and the recombination process in the NCs. But if the NCs are far from the nano-contact, the carriers recombination process affects less and less the

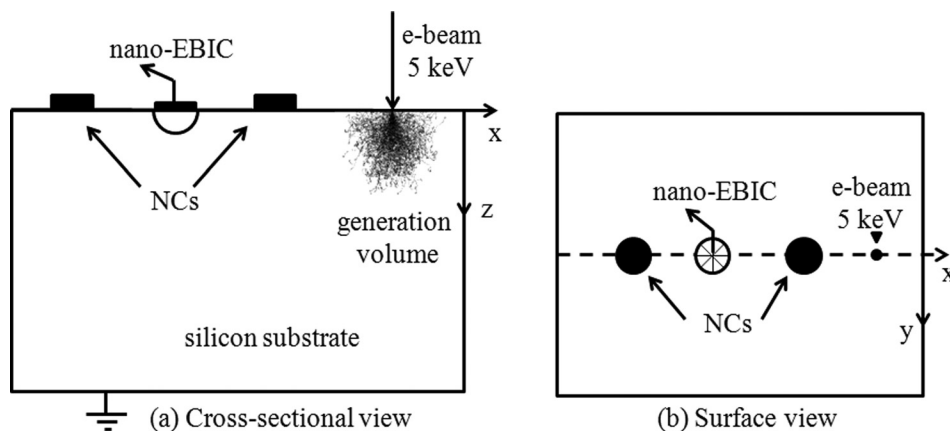


FIG. 1. A Schematic representation of the nano-EBIC procedure in the presence of two nanocrystals. (a) Cross-sectional view and (b) surface view.

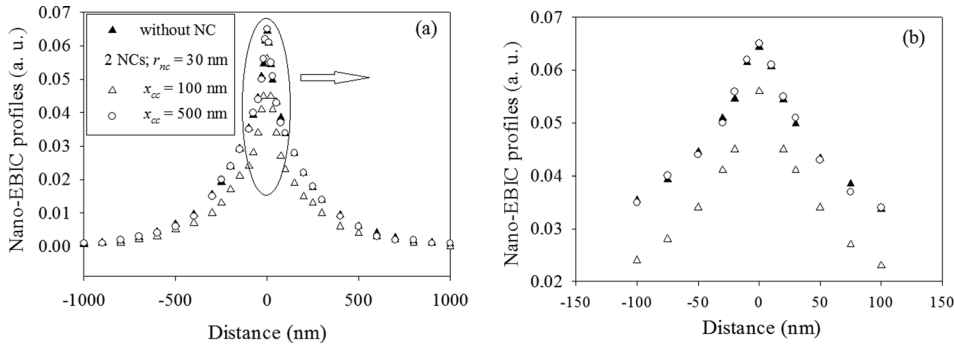


FIG. 2. (a) Simulated collection efficiency profiles of the nano-EBIC collected by a nano-contact in the absence and in the presence of two NCs nano-crystals for two values of x_{cc} = 100 and 500 nm to highlight the separating distance effect. (b) Enlargement of the nano-EBIC profiles central parts.

collected current, leading to an increase in the nano-EBIC. This is due to the fact that the nano-EBIC current is entirely controlled by the nano-depletion zone, since each generated charge reaching this zone is collected to contribute to the nano-EBIC. On the other hand, if we consider that x_{cc} indirectly represents d_{NC} , we can suppose that the carrier recombination efficiency becomes stronger for higher d_{NC} (for a lower x_{cc}). This assertion is consistent with previous experimental results.^{32,33}

Another interesting parameter can be also introduced here, namely, the surface recombination velocity v_s around the collecting nano-contact. When $v_s = 0$ near the collecting electrode, $\eta(x)$ presents a high profile, which corresponds to the absence of NCs around and close to the nano-contact or the NCs are located far away. But for $v_s > 0$, $\eta(x)$ takes a lower values indicating an increase in the carrier recombination process because the NCs are located close to the nano-contact.

Concerning the relationship between x_{cc} and d_{NC} , we assumed above that at a given analyzed surface a lower value of x_{cc} corresponds to a higher value of d_{NC} , and a higher x_{cc} corresponds to a lower d_{NC} . In this case, we can expect that if x_{cc} reaches a threshold value x_{th} , we obtain the same results than that obtained in the absence of the NCs at the studied surface. For this purpose, x_{cc} was varied from 40 nm to 1000 nm. Fig. 3 gives the variation of the collection efficiency maximum η_{max} (the right axis) as a function of x_{cc} . As

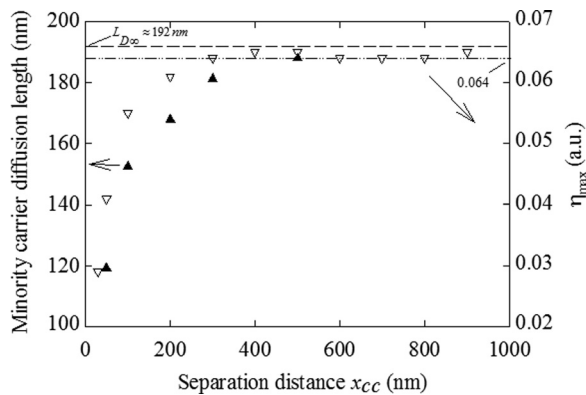


FIG. 3. The right axis: Monte-Carlo simulated maximum collection efficiency η_{max} versus x_{cc} in the presence of two NCs located around the collecting nano-contact in a linear arrangement in the e-beam irradiation trajectory. The curve is well fitted by $\{1 - \exp(-x_{cc}/x_0)\}$. The left axis: The minority carrier diffusion length (L_D) as a function of the distance (x_{cc}) separating the two NCs from the collecting nano-contact. For $x_{cc} = x_{th}$, L_D reaches a plateau, in which the value corresponds to that obtained in the absence of NCs.

x_{cc} increases, η_{max} increases and reaches a maximum value of $\eta_{max} = 0.064$ for $x_{th} \approx 400$ nm. The same value was obtained on the condition of the absence of NCs as can be shown in Figures 2(b) and 3. This result leads to suggest that at a distance greater than $x_{th} \approx 400$ nm around of the nano-contact the presence of NCs has no effect on the induced current. Moreover, we notice that $\eta_{max}(x_{cc})$ is well fitted by the standard growth exponential law

$$\eta_{max}(x_{cc}) \propto [1 - \exp(-x_{cc}/x_0)], \quad (2)$$

where $x_0 \approx 50$ nm is extracted from the fitting procedure.

The parameter x_0 can be defined as the distance from which the charge collection ability of the nano-contact is lessened and therefore can be neglected. In this case, we can determine an areal zone (or a “collection-cross section”) which may characterize the charges attraction strength of the nano-contact. Seeing that η_{max} represents the ability of the nano-contact to collect a generated charge located at its center, we define a “collection cross-section” characterizing the attraction strength by the nano-contact of a charge located around it. On other words, this collection cross-section represents the sensitive area around the nano-contact. Therefore, the cross-section shape is annular whose radius is defined by x_{cs} from the edge of the nano-contact. Since x_{cc} is measured from the center of the nano-contact to the center of each NC, we define x_{cs} by $x_{cs} = x_0 - (r_D + r_{NC}) = 10$ nm. In this case, the collection cross-section is equal to $\pi \times [(x_{cs} + r_D)^2 - r_D^2] = 300 \times \pi \text{ nm}^2$. This is the surface of the ring area surrounding the nano-contact at the sample surface. This areal value is equal to the surface of the nano-contact with its depletion zone ($2 \times \pi \times r_D^2 + \pi \times r_D^2 = 300 \times \pi \text{ nm}^2$). This corroborates the significance of the collection cross-section which would represent the collection ability of the hemispherical nano-contact in a bi-dimensional shape.

Concerning x_{th} , we think that the value of $x_{th} \approx 400$ nm is underestimated. Indeed, we did not take into account of the nano-depletion established between both NCs and the sample surface. We think that this nano-depletion also affects the nano-EBIC process leading a reduction of $\eta(x)$ even for distances higher than $x_{th} \approx 400$ nm. We also neglected the overlapping of the potential between NCs and the nano-contact for weak x_{cc} .

As quoted above, the variation of x_{cc} leads to the variation of the nano-EBIC profile. As a consequence, the minority carriers effective diffusion length (L_D) is also affected as shown in Fig. 3 (the left axis). Let us notice that L_D is called

effective diffusion length, which is different from the bulk (real) diffusion length L_B , because many parameters (nano-contact size, depletion size, e-beam energy) affect its extraction from the nano-EBIC profiles.^{15,19} The values of L_D were extracted from the fitting curves of the nano-EBIC profiles by the empirical law $\exp(-x/L_D)$. As the distance x_{cc} increases, L_D increases then saturates at $L_{D\infty} \approx 192$ nm for large values of x_{cc} . This last value is also obtained in the absence of NCs at the studied surface. Therefore, the location of the NCs from the collecting nano-contact controls the shape (the variation of L_D) and the amount (η_{max}) of the nano-EBIC profiles.

All these results give incontestably interesting information describing the NCs effects on the nano-EBIC, the diffusion length, and the surface recombination process in the area around and close to the collecting nano-contact. Even if x_{cc} may describe d_{NC} effects, it would be interesting to simulate separately the effects of NCs density and size. Indeed, in some previous experimental works, it was shown that both NCs parameters can affect memory and optoelectronic devices,^{32,33} but it was difficult to distinguish between the specific effects of size and density. The Monte-Carlo simulation would give supplementary information on both parameters.

IV. CONCLUSION

The nano-EBIC collection efficiency was analyzed by the use of the Monte-Carlo simulation. For the calculation, we took into account the effects of two uncapped NCs, located around a collecting nano-contact in a linear and symmetrical arrangement along the e-beam irradiation trajectory. The surface recombination velocity was taken equal to zero at the free surface, and the NCs were considered as recombination centers. The main parameter, which was varied to highlight the effects of the NCs presence, is the distance separating each NC from the collecting nano-contact. This parameter was shown to be related to the NCs density. A threshold value from which the NCs presence has no effect on the nano-EBIC was found to be equal to $x_{th} \approx 400$ nm. This value was underestimated because the nano-depletion zone under each NC was neglected in our simulation. On the other hand, η_{max} versus x_{cc} represents an exponential law leading to the determination of a collection cross-section, which characterizes the ability of the nano-contact to trap generated charges. The minority carrier diffusion length L_D was found to be increasing with x_{cc} until a saturation value equal to that obtained in the absence of the NCs.

Finally, this simulation study gives important information on the presence of the NCs around a collecting nano-contact. The region around the collecting nano-contact is

very sensitive and any process occurring in this area affects the collected current. This study emphasizes the ability of the nano-EBIC to characterize nanostructures thanks to its sensitivity.

- ¹L. Jastrzebski, J. Lagowski, and H. C. Gatos, *Appl. Phys. Lett.* **27**, 537 (1975).
- ²H. J. Leamy, *J. Appl. Phys.* **53**, R51 (1982).
- ³J. Boersma, J. J. E. Indenkleef, and H. K. Kuiken, *J. Eng. Math.* **18**, 315 (1984).
- ⁴C. Donolato, *Solid-State Electron.* **28**, 1143 (1985).
- ⁵D. Cavalcoli, A. Cavallini, and A. Casaldini, *J. Appl. Phys.* **70**, 2163 (1991).
- ⁶D. S. H. Chan, V. K. S. Ong, and J. C. H. Phang, *IEEE Trans. Electron Devices* **42**, 963 (1995).
- ⁷L. Chernyak, A. Osinsky, H. Temkin, J. W. Yang, Q. Chen, and M. Asif Khan, *Appl. Phys. Lett.* **69**, 2531 (1996).
- ⁸K. L. Luke, *J. Appl. Phys.* **90**, 3413 (2001).
- ⁹V. K. S. Ong and D. Wu, *IEEE Trans. Electron Devices* **48**, 332 (2001).
- ¹⁰L. Chernyak, A. Osinsky, and A. Schulte, *Solid-State Electron.* **45**, 1687 (2001).
- ¹¹S. Q. Zhu, E. I. Rau, and F. H. Yang, *Semicond. Sci. Technol.* **18**, 361 (2003).
- ¹²O. Kurniawan and V. K. S. Ong, *IEEE Trans. Electron Devices* **53**, 2358 (2006).
- ¹³M. Troyon and K. Smaali, *Appl. Phys. Lett.* **90**, 212110 (2007).
- ¹⁴K. Gacem, A. El Hdiy, M. Troyon, I. Berbezier, and A. Ronda, *Nanotechnology* **21**, 065706 (2010).
- ¹⁵Q.-T. Doan, A. El Hdiy, and M. Troyon, *J. Appl. Phys.* **110**, 024514 (2011).
- ¹⁶A. Marchand, A. El Hdiy, M. Troyon, G. Amiard, A. Ronda, and I. berbezier, *Appl. Phys. Lett.* **100**, 163117 (2012).
- ¹⁷M. Ledra and N. Tabet, *Superlattices Microstruct.* **45**, 444 (2009).
- ¹⁸M. Ledra and N. Tabet, *Int. J. Nano Biomater.* **2**, 307 (2009).
- ¹⁹Q. T. Doan, A. El Hdiy, and M. Troyon, *J. Appl. Phys.* **110**, 124515 (2011).
- ²⁰N. Ounissi, M. Ledra, and N. Tabet, *Int. J. Nanopart.* **6**, 232 (2013).
- ²¹Q. T. Doan and A. El Hdiy, *J. Appl. Phys.* **117**, 115704 (2015).
- ²²M. J. Berger and S. M. Selzer, in *Studies in Penetration of Charged Particles in Matter*, edited by V. Fano (National Academy of Sciences, National Research Council, 1967), Publication No. 1133, Chap. 10.
- ²³G. Love, M. G. C. Cox, and V. D. Scott, *J. Phys. D: Appl. Phys.* **10**, 7 (1977).
- ²⁴L. Reimer and D. Stelter, *Scanning* **8**, 265 (1986).
- ²⁵D. E. Newbury, D. C. Joy, P. Echlin, C. E. Fiori, and J. I. Goldstein, *Advanced Scanning Electron Microscopy and X-Ray Microanalysis* (Plenum Press, New York, 1986).
- ²⁶D. C. Joy, in the *Proceeding of European Meeting on Electron Microscopy*, edited by A. J. Craven and H. Elder (Inst. of Physics, London) [Inst. Phys. Conf. Ser. **93**, 23 (1988)].
- ²⁷D. C. Joy and S. Luo, *Scanning* **11**, 176 (1989).
- ²⁸D. C. Joy, *Scanning Microsc.* **5**, 329 (1991).
- ²⁹R. Shimizu and Z. J. Ding, *Rep. Prog. Phys.* **55**, 487 (1992).
- ³⁰N. Tabet and M. Ledra, *Mater. Sci. Eng. B* **42**, 181 (1996).
- ³¹M. Ledra and N. Tabet, *J. Phys. D: Appl. Phys.* **38**, 3845 (2005).
- ³²A. El Hdiy, K. Gacem, M. Troyon, A. Ronda, F. Bassani, and I. Berbezier, *J. Appl. Phys.* **104**, 063716 (2008).
- ³³P. F. Lee, X. B. Lu, J. Y. Dai, H. L. W. Chan, E. Jelenkovic, and K. Y. Tong, *Nanotechnology* **17**, 1202 (2006).